



Hot cracking in autogenous welding of 6061-T6 aluminum alloy by rectangular pulsed Nd:YAG laser beam

Hossain Ebrahimzadeh¹ · Hassan Farhangi¹ · Seyed Ali Asghar Akbari Mousavi¹

Received: 15 October 2019 / Accepted: 25 March 2020 / Published online: 24 April 2020
© International Institute of Welding 2020

Abstract

Due to high hot crack susceptibility of Al-Mg-Si alloys, autogenous welding by rectangular pulsed laser beam has not been generally successful in the removal of cracks. In this research, the effect of pulsed Nd:YAG laser parameters and preheating on the creation of hot cracks in the 6061-T6 aluminum alloy was investigated. The sample that was fabricated by the laser parameters including 1 Hz, 0.12 mm/s, 10 ms, and without preheating exhibited the highest cooling rate and the smallest dendrite arm spacing but no hot crack was observed. The tensile test specimens of this sample fractured at a point far from the weld metal and a decrease in the precipitation of silicon and magnesium in the inter-dendritic space and the reduction of thermal stresses resulted in the elimination of hot cracks. However, according to macro-scale models for the creation of hot cracks, preheating decreased the tensile stresses in the BTR (brittle temperature range), but increasing the preheating temperature led to increasing rather than decreasing the hot crack length. In this case, the formation of hydrogen porosity, the segregation of silicon and magnesium, and the creation of low melting point compounds were the important parameters affecting the hot crack initiation and growth.

Keywords 6061 aluminum alloy · Laser welding · Hot crack modeling · Solidification microstructure · Rectangular pulse · Stress simulation

1 Introduction

Aluminum-magnesium-silicon alloys, which are known as 6XXX Al alloys, are one of most widely used alloys in industry [1, 2]. High coefficients of thermal expansion, the formation of low melting temperature compounds, and a great difference between solidus and liquidus temperatures increase the possibility of the formation of hot cracking in aluminum-magnesium-silicon alloys during fusion welding [3–5]. Owing to the susceptibility of 6XXX series to hot cracks, solid-state welding processes, especially the friction stir welding method, have been paid attention [6, 7]. Of the fusion methods that are being used to join 6XXX series, the gas metal

arc welding method using dissimilar filler metals such as 4043 and 5356 aluminum alloys as well as the electric resistance welding method can be mentioned [8–10]. Considering the applications of 6XXX series in corrosive environments, the chemical composition mismatch after welding through fusion methods along with the presence of a dissimilar filler metal enhances galvanic corrosion in corrosive environments [11–13] and also, yield strength, tensile strength, and elongation of the weld metal will be lower than those of the base metal [4, 14, 15]. Therefore, fusion welding without using dissimilar filler metals is an interesting topic. The studies show that conventional fusion methods have been almost unsuccessful to inhibit the formation of hot cracking during the welding of 6XXX series. Hence, recently, many investigations have been performed in order to reduce hot cracking using high-density sources such as laser beam as well as innovative techniques to weld these alloys [16–18]. In the cases which have led to the removal of cracks using a pulsed laser beam, the mode of ramp-down laser pulse has been used. In these studies, it has been noted that the removal of hot cracking is not possible due to the high rate of solidification in rectangular pulses which are available in most of the laser welding machines [19–21]. Although using the mode of ramp-down laser

Recommended for publication by Commission IX - Behaviour of Metals Subjected to Welding

✉ Hossain Ebrahimzadeh
h.ebrahimzadeh@ut.ac.ir

¹ School of Metallurgy and Materials Engineering, College of Engineering, University of Tehran, P.O. Box 11155-4563, Tehran, Iran

pulse has resulted in a substantial decrease in the dimensions of hot cracks, some other researchers have mentioned the presence of residual micro-cracks in weldments [22].

There are micro-, meso-, and macro-scale models for the prediction of hot cracks. In the micro-scale, the solidification microstructure and the solid/liquid interface are important. In this scale, the RDG (Rappaz Drezet Gremaud) model and other criteria such as the Kou's hot crack criterion based on the melt flow in the interdendritic spaces and the balance of melt feeding and consumption formulate the susceptibility to hot cracking. The results of the related research works show that decreasing the solidification rate and the strain rate and increasing the temperature gradient lead to reducing hot cracks. Also, increasing the dimensions of the solidification microstructure, due to the enlargement of the melt flow canals, improves the melt feeding and thus reduces hot cracking [23–26]. Macro-scale models also predict the susceptibility to hot cracking based on stress, strain, or the strain rate that enters the solidifying melt. For example, the results of some studies have shown that preheating reduces the stresses in the brittle temperature range (BTR) and therefore reduces hot cracking [27]. It should be noted that BTR is the temperature range of the solidification end in which hot cracking is most likely to occur.

In this research, the effect of Nd:YAG laser parameters with a rectangular pulse and using preheating on the formation of hot cracks as well as finding a relationship between solidification microstructure of the weld, the base metal microstructure and hot cracks have been investigated.

2 Experimental procedure

A commercial aluminum-magnesium-silicon alloy sheet, AA6061, with a thickness of 0.8 mm was welded using 80 W, Nd:YAG pulsed laser machine in the form of bead-on-plate and partial penetration. The heat treatment conducted on the 6061 aluminum alloy was T6 (solution treatment at 530 °C for 35 min, quenching in the water and aging at 160 °C for 18 h). The chemical composition of the alloy has been presented in Table 1. Preheating was carried out by an electrical resistance heating pad at 100, 200, and 300 °C, respectively. The welding parameters are displayed in Table 2.

In pulse laser welding, heat input, the average peak power (APP), and the average peak power density (APPD) are defined by the following formulas [28]:

$$\text{Heat input} \left(\frac{\text{J}}{\text{mm}} \right) = \frac{\text{frequency(Hz)} \times \text{pulse energy(J)}}{\text{welding speed} \left(\frac{\text{mm}}{\text{s}} \right)} \quad (1)$$

$$\text{Average Peak Power(W)} = \text{APP(W)} = \frac{\text{pulse energy(J)}}{\text{duration time(s)}} \quad (2)$$

$$\begin{aligned} \text{Average Peak power Density} \left(\frac{\text{W}}{\text{mm}^2} \right) \\ = \text{APPD} \left(\frac{\text{W}}{\text{mm}^2} \right) = \frac{\text{APP(W)}}{\text{spot area}(\text{mm}^2)} \end{aligned} \quad (3)$$

The results of the calculation of the abovementioned parameters have been presented in Table 2. The effects of the laser welding parameters and preheating on the formation of hot cracking were examined by an optical microscope as well as a scanning electron microscope (SEM). Keller's reagent was employed for etching by a modified technique [29]. The Clemex Image Analysis software was used to measure the grain size and the inter-dendritic spacing. Energy dispersive spectroscopy (EDS) was used to quantify the elements which precipitated in the inter-dendritic spaces. Tensile stresses caused by welding were simulated by the ANSYS APDL software. The dimensions of the samples simulated were $100 \times 20 \times 0.8 \text{ mm}^3$. The meshes were of quad type and their size was $1 \times 1 \times 0.4 \text{ mm}^3$. The thermal source was heat flux so that it was assumed a heat element transfers energy of each pulse in a circular area with a diameter equal to the laser beam at a time equal to the laser duration time to the workpiece surface. 3D heat conduction, radiation, and convection were considered. In addition, it was assumed that the two end of the sample were fixed. Tensile test specimens were fabricated according to the ASTM E8 standard with sub-size dimensions (Fig. 1) and they were transverse to the weld line. They were tested at a loading rate of 1 mm/min. Prior to performing the tensile test, solution and aging heat treatments of tensile test specimens were carried out according to the ASTM B918-09 standard. Solution treatment at 530 °C for 35 min was carried out to solve the solutes in the aluminum matrix. The samples were quenched in water which was in the room temperature exactly after the solution treatment. The samples were aged at 160 °C for 18 h. Aging treatment is generally recognized to

Table 1 The chemical composition of 6061 aluminum alloy

Al Wt.%	Mg Wt.%	Si Wt.%	Cu Wt.%	Zn Wt.%	Mn Wt.%	Cr Wt.%	Fe Wt.%	Ti Wt.%	Ni Wt.%
Balance	0.91	0.69	0.22	0.06	0.05	0.16	0.43	0.05	0.01

Table 2 Laser welding parameters

Sample No.	Pulse energy (J)	Focal spot diameter (mm)	Frequency (Hz)	Duration time (ms)	Welding speed (mm/s)	Preheat (°C)	Heat input (J/mm)	Average peak power (kW)	Average peak power density (kW/mm ²)
1	4.8	0.5	1	10	–	–	–	–	–
2	4.8	0.5	4	2	0.50	–	38.4	2.4	12.2
3	4.8	0.5	4	4	0.50	–	38.4	1.2	6.1
4	4.8	0.5	4	6	0.50	–	38.4	0.8	4.1
5	4.8	0.5	4	8	0.50	–	38.4	0.6	3.1
6	4.8	0.5	4	10	0.50	–	38.4	0.48	2.4
7	4.8	0.5	1	10	0.50	–	9.6	0.48	2.4
8	4.8	0.5	4	10	0.25	–	76.8	0.48	2.4
9	4.8	0.5	1	10	0.12	–	38.4	0.48	2.4
10	4.8	0.5	1	8	0.12	–	38.4	0.6	3.1
11	4.8	0.5	4	10	0.50	100	38.4	0.48	2.4
12	4.8	0.5	4	10	0.50	200	38.4	0.48	2.4
13	4.8	0.5	4	10	0.50	300	38.4	0.48	2.4
14	4.8	0.5	1	10	0.12	300	38.4	0.48	2.4

cause the precipitation of Mg₂Si particles in the aluminum matrix.

3 Results

Figure 2a shows the top surface of sample no. 1 welded at 10 ms, 4.8 J pulse energy, and 1 Hz pulse frequency. Even in discrete pulses, there are star-type hot cracks in the center of the weld pool. Figure 2b shows the cross section of sample no. 9. The welding mode was bead-on-plate and partial penetration.

In Fig. 3, the effect of increasing the duration time on the dimensions of the hot cracks is depicted. Applying successive pulses, and thus forming the weld seam, leads to the conversion of the star crack to the longitudinal crack. The longitudinal cracks are created in the regions close to the weld axis. In this region, the highest tensile stress due to welding is created [30, 31]. As can be seen, with increasing the duration time, the crack length decreased so that the crack changed from a continuous form to isolated cracks.

For the investigation of welding speed and pulse frequency separately on the hot crack creation in three samples was fabricated (Fig. 4). Decreasing the welding speed caused

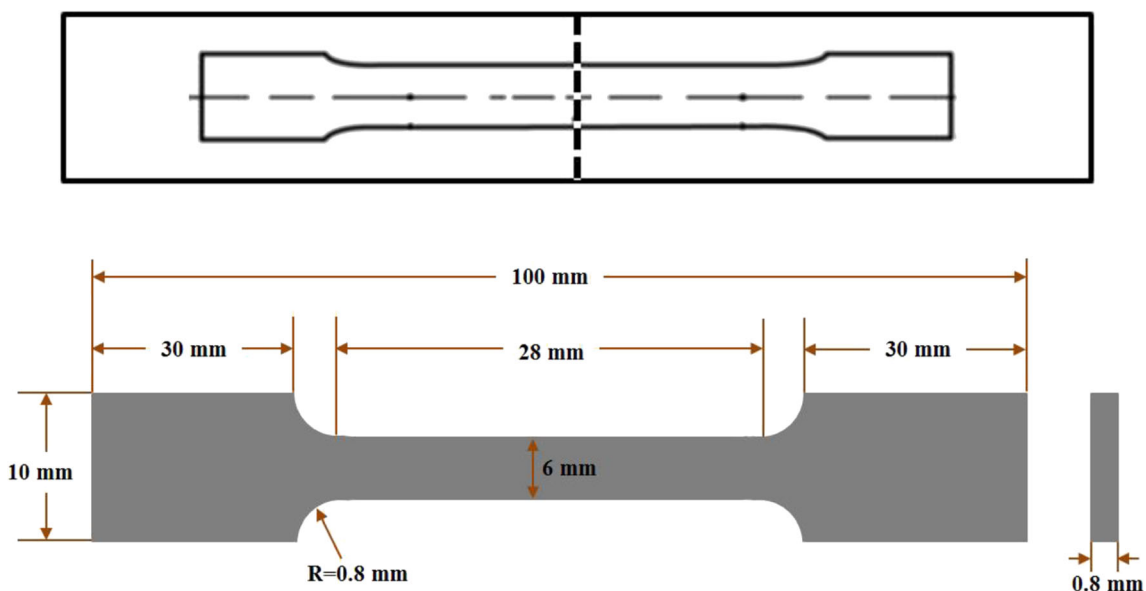


Fig. 1 The sample location relative to the weld line and the dimensions of the tensile test specimens

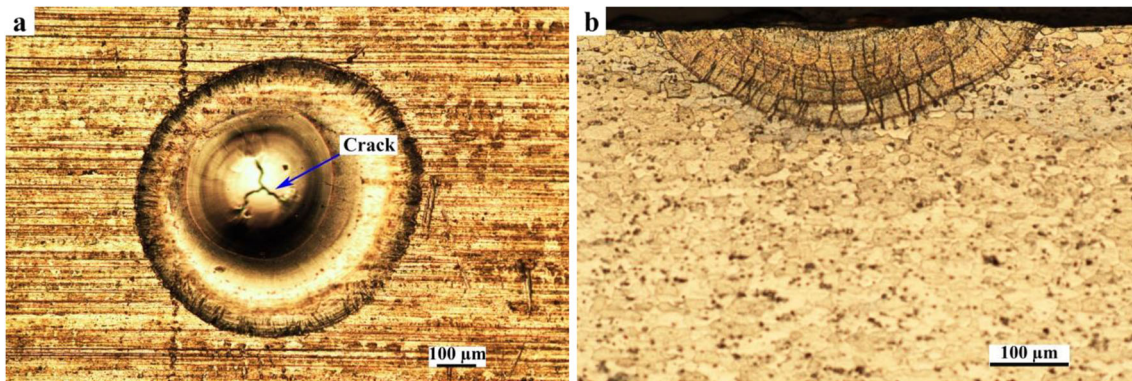


Fig. 2 **a** The top view of a single pulse. Star crack can be seen in the center of the weld pool. **b** The cross section of sample no. 9. The welding mode was bead-on-plate and partial penetration

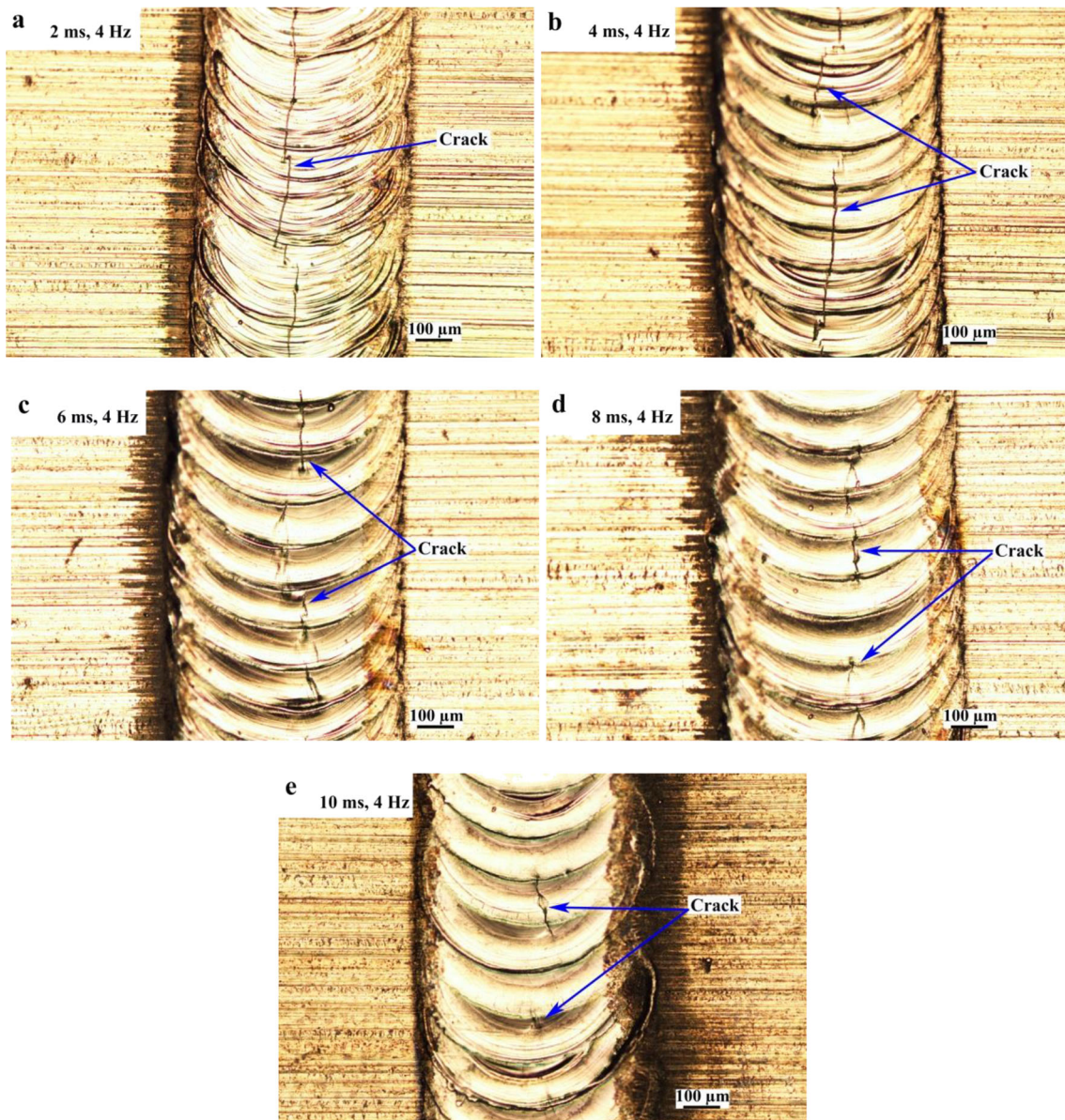


Fig. 3 The effect of the duration time on hot cracks. The pulse energy, welding speed, and focal spot diameter were 4.7 J, 0.50 mm/s and 0.5 mm, respectively. Increasing the duration time decreases hot cracks

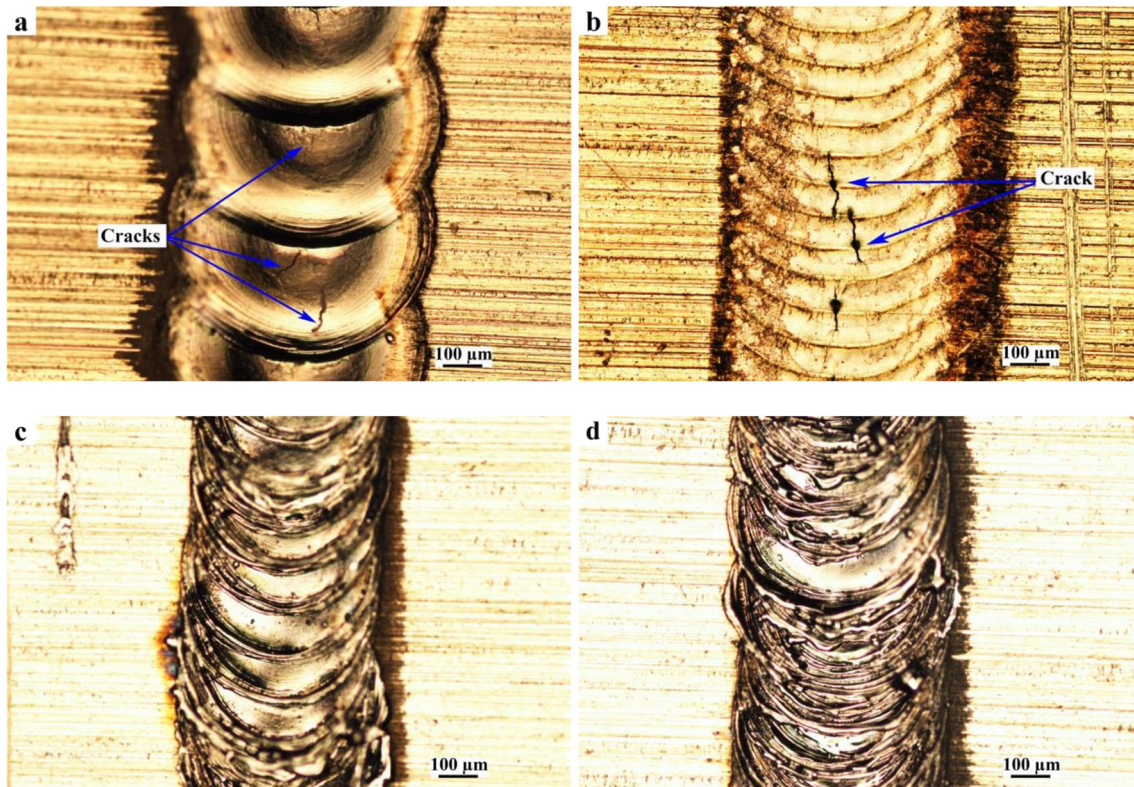


Fig. 4 The effect of welding speed and pulse frequency on the creation of hot cracks in samples no. 7 (a), no. 8 (b), no. 9 (c), and no. 10 (d). Only decreasing the welding speed and the pulse frequency simultaneously led to decreasing the hot crack

increasing the hot cracks compared with sample no. 6. Decreasing the laser frequency to 1 Hz and the welding speed to 0.12 mm/s had the most interesting effects on the reduction of hot cracking. Although the heat input was the same as that in the samples welded at 4 Hz and 0.5 mm/s (Table 2), the cracks were completely removed. The welding line profile is also indicative of the turbulence in the weld pool in this sample. The same results can be seen in sample no. 10 (Fig. 4). This weld has been fabricated at 1 Hz, 8 ms, and 0.12 mm/s. There is no crack at the top view of the sample.

Preheating was performed at 100, 200, and 300 °C. Figure 5 shows the effect of the preheating temperature on the solidification cracks. In the previous researches [18, 20, 32], it has been noted that hot cracking decreases with increasing the preheating temperature. Another reason for decreasing hot cracking by preheating the workpiece, which has been pointed out in the literature [4, 33–35], is decreasing the stresses applied to the weld pool during welding. Despite all the abovementioned reasons, all the preheated samples contained continuous cracks. Welding at 1 Hz created no continuous surface hot crack even under preheating at 300 °C. The samples exhibited smooth surface and there was no sign of high turbulence in the weld pool.

The microstructures of the welds are shown in Fig. 6. The inter-dendritic arm spacing of the non-preheated samples, i.e., samples no. 3, no. 6, and no. 9 were

0.77 μm, 0.94 μm, and 0.73 μm, respectively. Increasing the duration time caused increasing the inter-dendritic arm spacing and reducing both pulse frequency and welding speed together with each other caused decreasing inter-dendritic arm spacing. The spacing of the dendritic arms under preheating at 100 °C and 300 °C (samples no. 11 and no. 13) was 1.18 μm and 1.26 μm, respectively, which are higher than those in the samples without preheating. Increasing the preheating temperature led to increasing the inter-dendritic arm spacing. The dendrite arm spacing of sample no. 14 welded at the duration time of 10 ms, the pulse frequency of 1 Hz, and the preheating temperature of 300 °C was lower than that of sample no. 13. Decreasing the pulse frequency and the welding speed in the preheated sample caused a decrease in the dendrite arm spacing.

In Fig. 7, the linear EDS is shown. Due to the small size of dendrites, it is impossible to measure the elements in the dendrite boundaries. Therefore, the measurement was carried out in a linear form and changing the elements along the line was considered. The amounts of silicon and magnesium elements in the dendritic boundaries were higher than those in the matrix.

In the sections of the preheated samples, indications of hydrogen porosity were observed (Fig. 8).

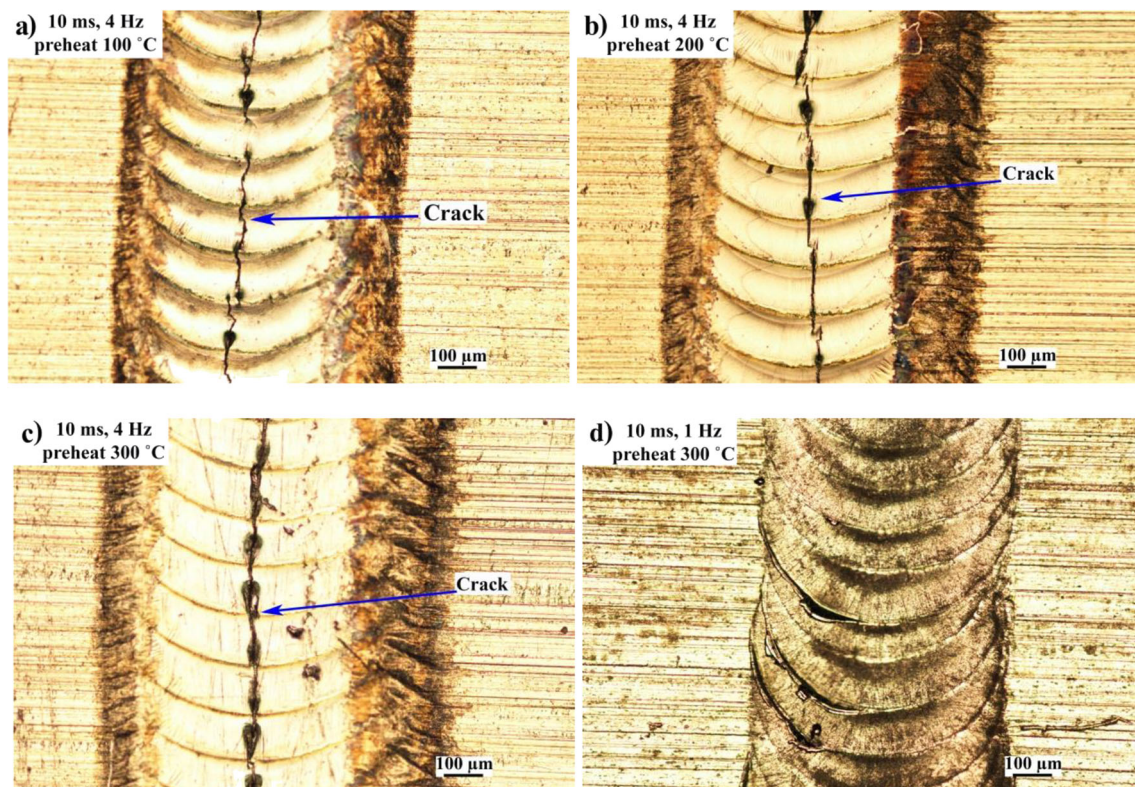


Fig. 5 The effect of preheating on the creation of hot crack. There is no longitudinal crack in sample no. 14 welded at 1 Hz

Figure 9 shows the tensile test results. As it is seen, samples no. 6 and no. 11 fractured from the weld metal. The strength of sample no. 6 is very low compared with that of samples no. 9 and no. 14. Figure 10 shows the SEM images of the fracture surfaces of the tensile test specimens.

4 Discussion

The heat input and therefore hot cracks will increase due to a lower welding speed and constant pulse frequency. Decreasing the pulse frequency at a constant welding speed caused lower pulse overlap, and therefore, crack healing by the next pulse cannot be carried out. To inhibit hot cracking, minimum overlapping is required.

The equation which approximately shows the strain rate is as follows [21]:

$$\dot{\epsilon} = -\beta_T \dot{T}_{SL} = \beta_T |G_{SL} R_{SL}| \quad (4)$$

where β_T is the coefficient of contraction, comprising solidification shrinkage and thermal expansion, \dot{T}_{SL} is the cooling rate at the solid/melt interface. In addition, decreasing $G \times R$ causes coarsening of the dendritic structure, and as a result, eases melt feeding and decreases the hot cracking susceptibility [21]. In general, the decrease in G and R causes coarsening

of the inter-dendritic spacing and increases the amount of feeding, while on the other hand, strain rate decreases according to Eq. (4). The temperature gradient in solidification (G_{SL}) is the temperature gradient relative to the location between the solidification interface and the center of the weld pool. In some literatures, the temperature gradient from the base metal is incorrectly taken into account [35]. Therefore, since the temperature of the solidification interface is the same as the melting point of the base metal, it can be concluded that everything that increases the temperature of the weld pool at a particular time will increase the temperature gradient. In some studies, $V \times \cos(\theta)$ (V is the welding speed and θ the angle between the solidification location and the welding line) is considered the solidification rate (R_{SL}) [35]. Nonetheless, it should be taken into account that in low frequency pulsed welding, each pulse is melted and solidified separately. Therefore, the welding speed cannot determine the solidification rate in pulsed welding. In Table 2, APP, APPD, and heat input for different samples are calculated. Except samples no. 7 and no. 8, all the other samples have been fabricated under the same heat input. Increasing the duration time decreases APP and APPD. Through the following formulas, the approximate effect of the duration time and preheating temperature on solidification rate and temperature gradient can be shown.

Suppose a heat element is attached to a metal surface that transfers Q energy to the surface with an area of A

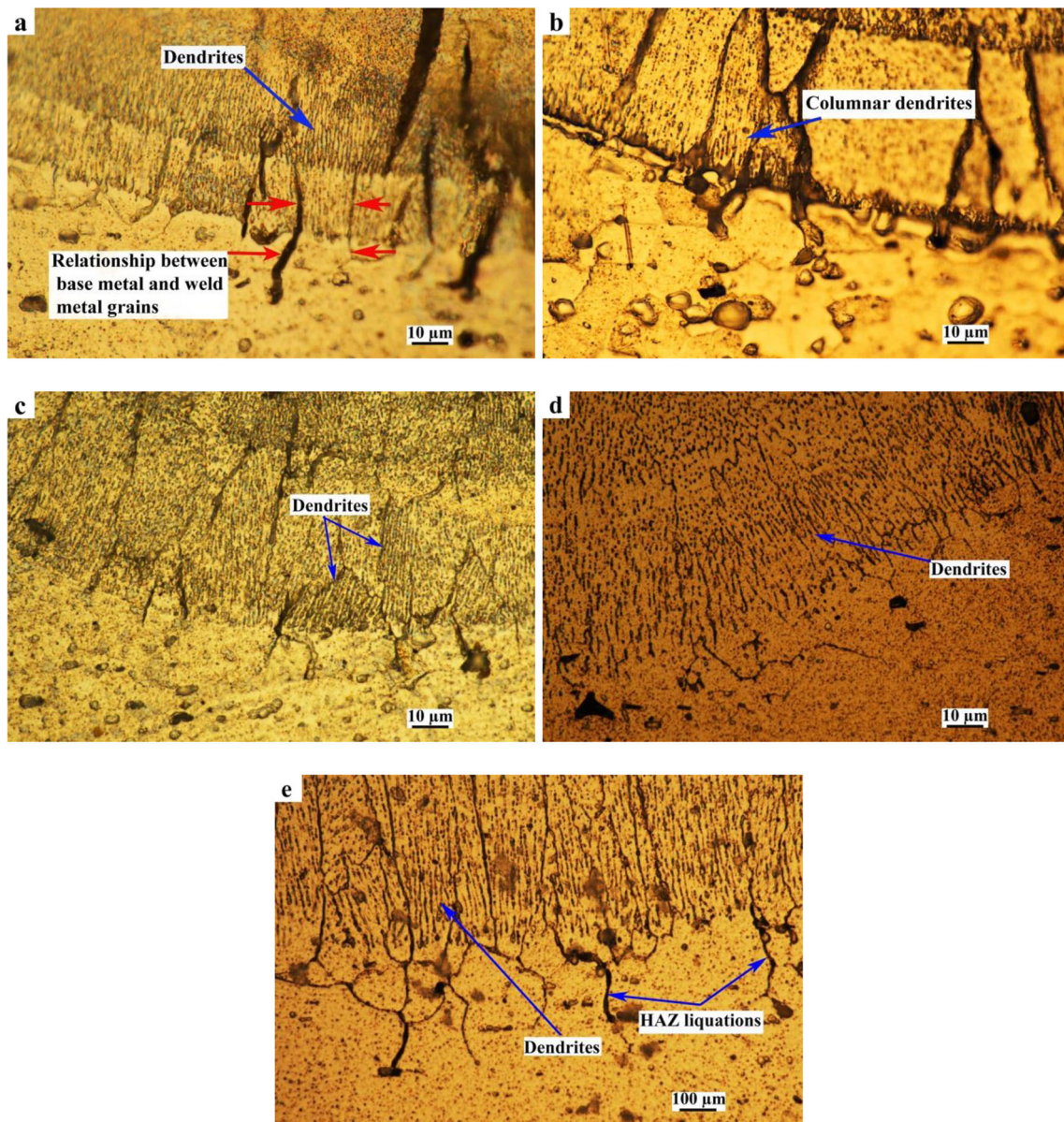


Fig. 6 The cross section of samples no. 3 (a), no. 6 (b), no. 9 (c), no. 13 (d), and no. 14 (e). Columnar dendrites and grains can be seen

during the duration time of t (Fig. 11). This heat creates a temperature gradient dT/dx at the depth of the workpiece. According to Fourier’s law of thermal conduction, it can be written:

$$\frac{Q}{t \times A} = -k \frac{dT}{dx} \tag{5}$$

where Q is heat, t is time, A is the surface at which heat is transferred, k is the heat transfer coefficient, and dT/dx is the temperature gradient. After the radiation reaches and heats the material surface, it can be assumed as a heat element that transfers heat to the metal. This heat element transfers an amount of heat equal to the laser pulse energy from a surface with an area equal

to the beam spot size to the workpiece at a period equal to the duration time. As a result:

$$\left(\frac{Q}{t \times A} = APPD\right) \Rightarrow -\frac{APPD}{k} = \frac{dT}{dx} \left(\frac{dT}{dx} = G \text{ and } k = \text{const.}\right) \Rightarrow G_{SL} \propto APPD \tag{6}$$

Figure 12 shows the effect of APPD on the temperature gradient of the weld pool and the base metal schematically. The peak power shows the amount of energy that is applied to the material at a constant duration time or constant energy in the desired pulse duration time. If a constant amount of energy is applied at a lower time, the material cannot disperse the heat immediately and the temperature of the irradiated region will

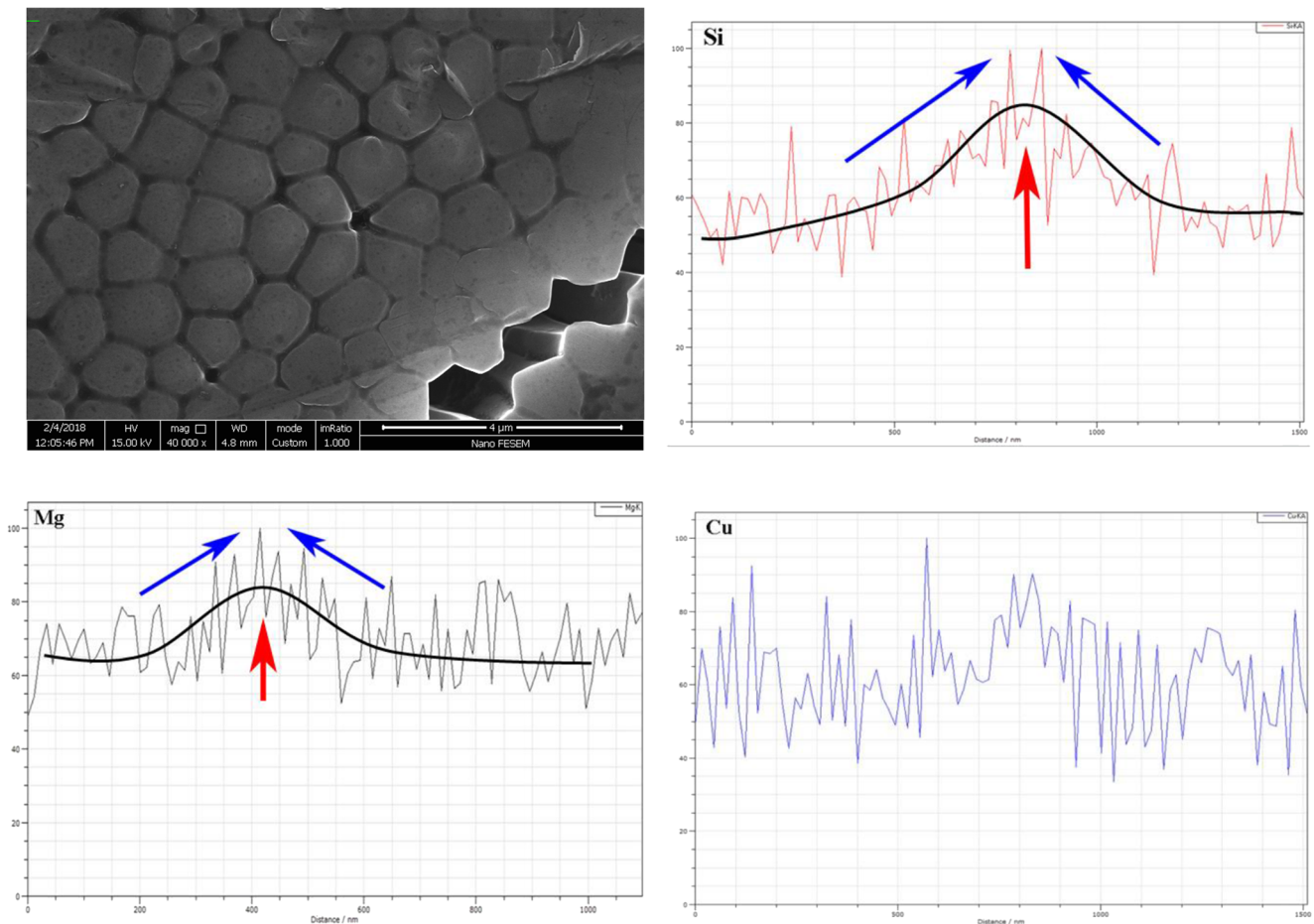


Fig. 7 The precipitation of Si and Mg alloying elements in the inter-dendritic spacing

increase. Because of very low duration time, laser pulse can melt the material with a very low amount of energy. Sometimes, at high duration times, laser pulse loses melting ability. With increasing the duration time, peak power decreases and this decrease, in turn, results in decreasing the maximum temperature that the weldment can reach ($\Delta T \downarrow$), and therefore, temperature gradient decreases. On the other hand, due to time consuming of heat transfer, at a high APPD, lower heat goes into the base metal at the same time

in a lower APPD, and therefore, the temperature gradient of the base metal will increase. Solidification rate is directly proportional to the heat that dissipates from the interface per unit time. High-rate heat transfer causes high-rate solidification. The heat transfer depends on the temperature gradient of the base metal. In addition, in previous researches, it has been shown that increasing the duration time results in decreasing both G and R [36, 37].

$$G_{\text{solid}} = \frac{T_{\text{interface}} - T_{\text{base}}}{\Delta x} \quad (T_{\text{interface}} = \text{melting temperature and } T_{\text{base}} = \text{Preheat temperature}) \Rightarrow G_{\text{solid}} \propto \frac{1}{\text{Preheat temperature}}$$

According Fig.7 $\Delta x \propto \frac{1}{\text{APPD}} \Rightarrow G_{\text{solid}} \propto \text{APPD}$ (7)

$$\text{Solidification Rate} = R \propto \text{The Heat transfer} = \frac{Q}{t \times A} = -k \frac{dT}{dx} \quad (k = \text{const.}) \Rightarrow R \propto G_{\text{solid}} \propto \text{APPD} \& 1/\text{Preheat temperature}$$

From the abovementioned statements, it can be deduced that increasing the duration time resulted in decreased G and R and consequently decreased strain rate. Of course, decrease

can be also understood from the coarsening of dendritic arms which, in turn, facilitates the melt feeding and decreases hot cracking.

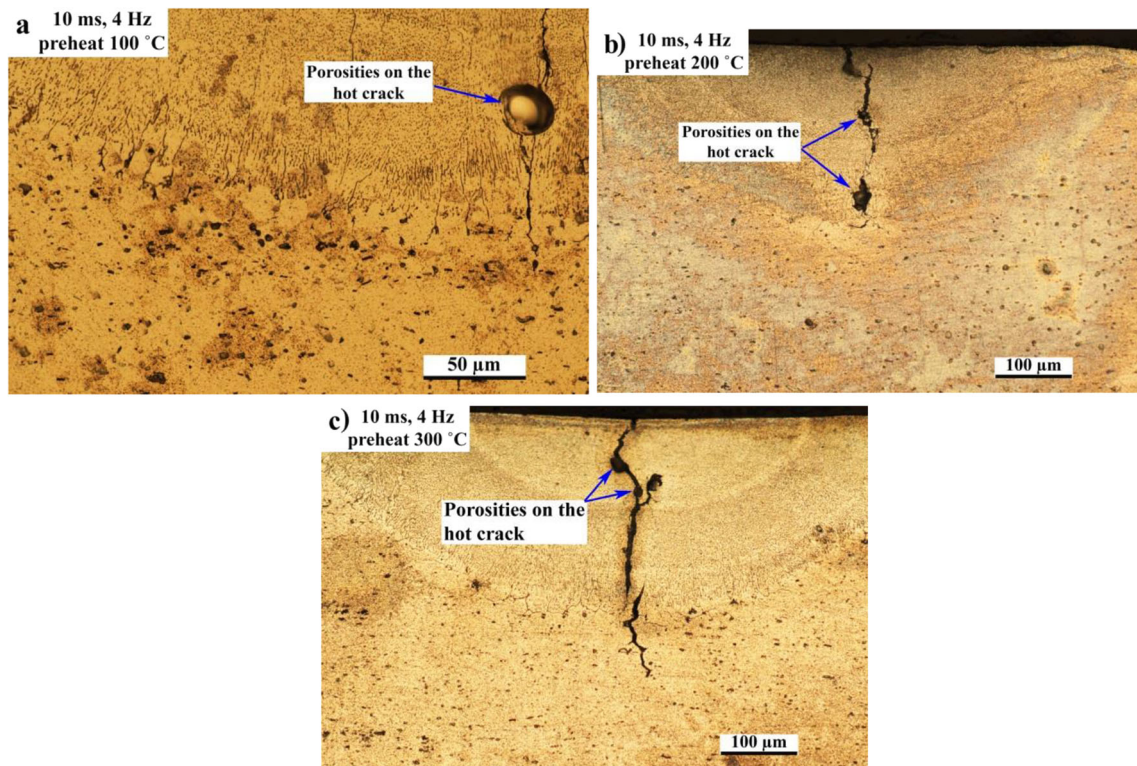
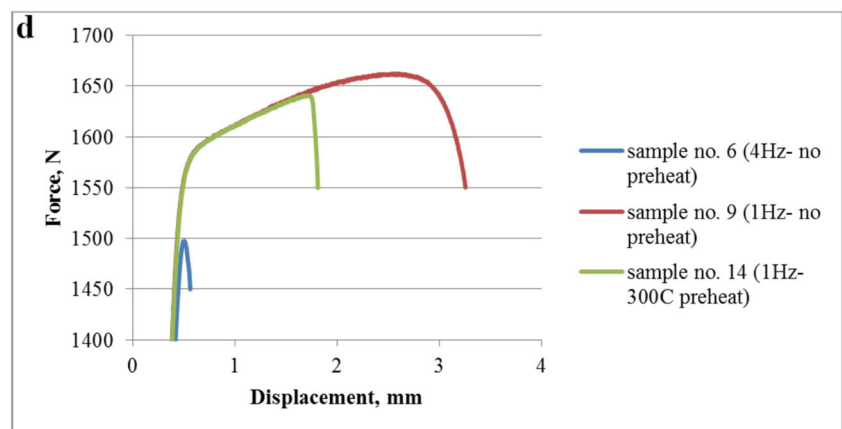
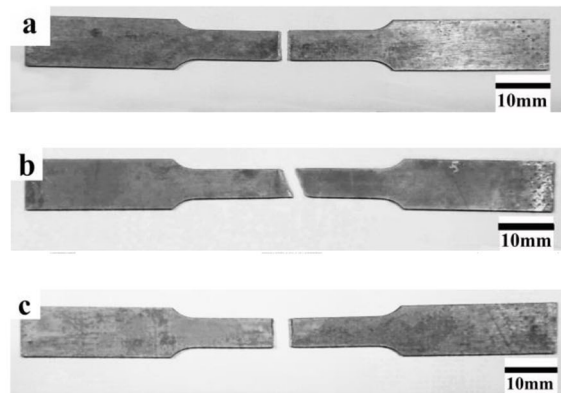


Fig. 8 Cross section of the preheated samples, i.e., samples no. 11, no. 12, and no. 13. Porosities can be seen on hot cracks

Fig. 9 **a** Sample no. 5 (4 Hz, no preheating). **b** Sample no. 6 (1 Hz, no preheating). **c** Sample no. 11 (1 Hz, preheating at 300 °C). **d** The tensile test result. It should be noted that since the weldment does not have full penetration, these results cannot be considered for the weld metal. In this study, these results are presented only for a qualitative comparison



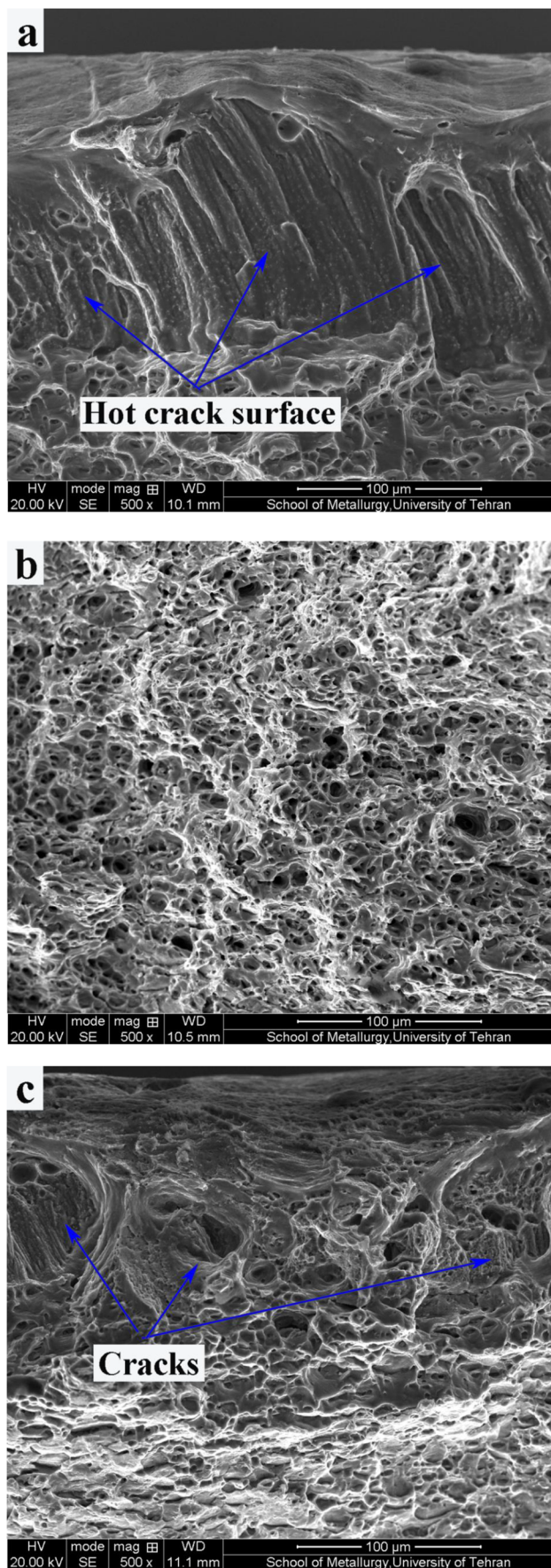


Fig. 10 The fracture surfaces of the tensile test samples. **a** Sample no. 6. **b** Sample no. 9. **c** Sample no. 14. The major part of the fracture surface in sample no. 6 can be related to the initial hot crack in the weldment. In sample no. 14, hot cracks are observed

In sample no. 9 welded at the pulse frequency of 1 Hz, the small size of the dendritic arms represented a large cooling rate ($G \times R$), and as a result, the values of R and G increased.

The appearance of the specimens welded at 1 Hz also shows that the temperature gradient in the weld pool was higher than that in all other specimens. Increasing the weld pool temperature gradient will increase the force required to stir the molten weld pool, including the Marangoni and Buoyancy forces, resulting in a greater turbulence in the weld pool [28].

However, hot cracks have completely disappeared. At 4 Hz, four pulses in each second and at 1 Hz, one pulse in each second is irradiated to the surface of the material. The time interval between two consecutive pulses at 4 Hz is 250 ms. At 1 Hz, there is enough time to cool the previous pulse and to dissipate heat from the pulse position, so that when the next pulse is irradiated, there is no previous accumulated heat in the welding position. The small amount of heat accumulation can also be understood from the small heat affected zone (HAZ) (Fig. 6). The liquated zone area in the HAZ is smaller than the samples welded at the pulse frequency of 4 Hz and/or preheated. This will reduce the welding tensile stress that causes decreased hot cracking. The maximum Von-Mises stress simulated for samples no. 6 (4 Hz) and no. 9 (1 Hz) in the weld center was 157 MPa and 79 MPa, respectively. These two samples had equal heat inputs. In fact, solidification shrinkage and thermal shrinkage cause stresses on the weld pool. Solidification shrinkage totally depends on the alloy nature while thermal shrinkage depends on the peak temperature, temperature gradient, and the volumes of the weld metal and base metal which are subjected to the welding heat.

Decreasing R and G_{solid} and thus decreasing the cooling rate and coarsening of the structure in the preheated samples did not only reduce hot cracks, but also increase them.

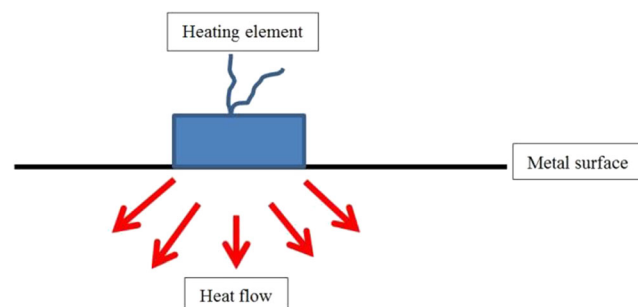
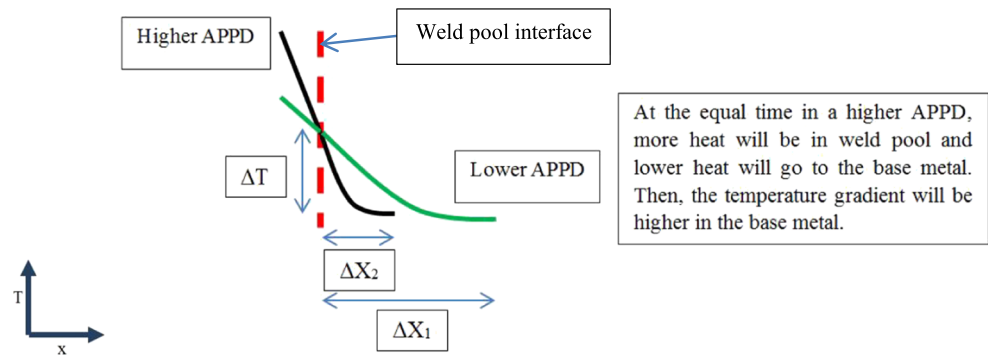


Fig. 11 The schematic illustration of heat transfer under a thermal element

Fig. 12 The effect of APPD on the temperature gradient of the base metal



The smooth appearance of the welds, as previously described, shows a calm pool and consequently a lower temperature gradient.

In a previous research, it has been also mentioned that the segregation of silicon and magnesium in the weld grain boundaries of AA6061 occurred. In this research, high segregation of silicon, low segregation of magnesium, and no segregation of copper have been reported [38]. The same results about the segregation of silicon and magnesium in the interdendritic arm spacing can be seen here. Magnesium and silicon form low-temperature eutectic compounds [39]. These eutectic compounds facilitate hot cracking. It is well known that high-rate solidification inhibits pushing back of the alloying elements. Decreasing the solidification and cooling rate at preheated samples cause the higher segregation [40–42] of these elements and higher hot cracks. It is another reason for removing cracks in sample no. 9. A high cooling rate in this sample caused decreased segregation of silicon and magnesium. It should be noted that the ratio of hydrogen solubility in melt to solid was 20:1. Decreasing the solidification rate causes hydrogen to escape from the melt and to create some bubbles [21, 43]. These bubbles act as the initiation sites for hot cracking and thus facilitate crack nucleation. The bubbles also decrease the material strength and facilitate the growth of hot cracks.

Since the weakest region fractures in the tensile test specimen, tensile test was performed to ensure that there was no crack in the weld line. It should be noted that since the weldment does not have full penetration, these results cannot be considered for the weld metal. In this study, these results are presented only for a qualitative comparison. Because the weld line exhibited a solidification microstructure with lower hardness and strength than those of the base metal, the samples underwent the age-hardening heat treatment before the tensile test. Therefore, the only reason for the decreased strength of the tensile test specimens was the presence of cracks in the microstructure. The specimen, in which the base metal fractured, showed small dimples indicating ductile fracture. The fracture surface of the specimen that contained cracks underwent no noticeable deformation.

Several tiny ties are observed on the crack which indicates weak bonding between the two surfaces of the crack. The sample that has been welded at 1 Hz and a preheating temperature of 300 °C (sample no.14) had some brittle areas and cracks. The SEM images are in good agreement with the tensile test results. The sample with the fracture surface containing dimples exhibited the highest strength and elongation. The presence of cracks in the sample preheated and welded at 1 Hz reduced the strength and the elongation.

5 Conclusions

In this research, the influences of the pulsed Nd:YAG laser parameters and preheating on the formation of hot cracks were investigated and it was deduced that the removal of hot cracking was possible by rectangular pulses. Etching the dendrites in this research resulted in obtaining good guides about the relationship between microstructure and hot cracking. The main conclusions of this study are as follows:

1. Increasing the duration time to 10 ms resulted in decreasing hot cracking. Reducing the pulse frequency to 1 Hz led to the complete removal of the cracks. Increasing the preheating temperature resulted in increased hot cracking.
2. Contrary to the existing micro- and meso-scale models, dendrite size, solidification rate, thermal gradient, and grain size are not the only parameters that affect the creation of hot cracks. In this regard, the precipitation of low-temperature eutectic compounds, the thermal stresses caused by the temperature distribution in the welding position, and the formation of hydrogen porosities caused by the welding parameters and increasing the preheating temperature should be taken into consideration.

Acknowledgments The authors would like to thank the metallography lab of the School of Metallurgy and Materials Engineering, University of Tehran.

References

- Davis JR (1993) ASM specialty handbook: aluminum and aluminum alloys. ASM International
- Zhang YM, Pan C, Male AT (2000) Improved microstructure and properties of 6061 aluminum alloy weldments using a double-sided arc welding process. *Metall Mater Trans A* 31A
- Ambriz RR, Mesmacque G, Ruiz A, Amrouche A, López VH (2010) Effect of the welding profile generated by the modified indirect electric arc technique on the fatigue behavior of 6061-T6 aluminum alloy. *Mater Sci Eng A* 527
- Handbook AM (1992) Welding brazing and soldering. ASM International, Cleveland
- Soysal T, Kou S (2018) A simple test for assessing solidification cracking susceptibility and checking validity of susceptibility prediction. *Acta Mater* 143:181–197
- D'Urso G, Giardini C, Lorenzi S, Pastore T (2014) Fatigue crack growth in the welding nugget of FSW joints of a 6060 aluminum alloy. *J Mater Process Technol*
- Abdulstaar MA, Al-Fadhalah KJ, Wagner L (2017) Microstructural variation through weld thickness and mechanical properties of peened friction stir welded 6061 aluminum alloy joints. *Mater Charact* 126:64–73
- Society AW (1997) Structural welding code aluminum. AWS Structural Welding Committee
- Florea RS, Solanki KN, Bammann DJ, Baird JC, Jordon JB, Castanier MP (2012) Resistance spot welding of 6061-T6 aluminum: failure loads and deformation. *Mater Des* 34
- Viveros KC, Ambriz RR, Amrouche A, Talha A, García C, Jaramillo D (2014) Cold hole expansion effect on the fatigue crack growth in welds of a 6061-T6 aluminum alloy. *J Mater Process Technol*
- Mujibur Rahman ABM, Kumar S, Gerson AR (2007) Galvanic corrosion of laser weldments of AA6061 aluminium alloy. *Corros Sci* 49
- Zhang DQ, Li J, Joo HG, Lee KY (2009) Corrosion properties of Nd:YAG laser–GMA hybrid welded AA6061 Al alloy and its microstructure. *Corros Sci* 51
- Rahman ABMM, Kumar S, Gerson AR (2010) The role of silicon in the corrosion of AA6061 aluminium alloy laser weldments. *Corros Sci* 52
- Vargas JA, Torres JE, Pacheco JA, Hernandez RJ (2013) Analysis of heat input effect on the mechanical properties of Al-6061-T6 alloy weld joints. *Mater Des* 52
- Chu Q, Bai R, Jian H, Lei Z, Hu N, Yan C Microstructure, texture and mechanical properties of 6061 aluminum laser beam welded joints. *Mater Charact*
- Kim DY, Park YW (2012) Weldability evaluation and tensile strength estimation model for aluminum alloy lap joint welding using hybrid system with laser and scanner head. *Trans Nonferrous Metals Soc China* 22
- Schneider A, Avilov V, Gumenyuk A, Rethmeier M (2013) Laser beam welding of aluminum alloys under the influence of an electromagnetic field. *Phys Procedia* 41
- Bergmann JP, Bielenin M, Stambke M, Feustel T, Witzendorff PV, Hermsdorf J (2013) Effects of diode laser superposition on pulsed laser welding of aluminum. *Phys Procedia* 41
- Zhang J, Weckman DC, Zhou Y (2008) Effects of temporal pulse shaping on cracking susceptibility of 6061-T6 aluminum Nd:YAG laser welds. *Weld J* 87:18–30
- Sheikhi M, Malek Ghaini F, Assadi H (2015) Prediction of solidification cracking in pulsed laser welding of 2024 aluminum alloy. *Acta Mater* 82:12
- Witzendorff PV, Kaierle S, Suttmann O, Overmeyer L (2015) In situ observation of solidification conditions in pulsed laser welding of AL6082 aluminum alloys to evaluate their impact on hot cracking susceptibility. *Metall Mater Trans A* 46A:11
- von Witzendorff P, Kaierle S, Suttmann O, Overmeyer L (2016) Monitoring of solidification crack propagation mechanism in pulsed laser welding of 6082 aluminum. In: SPIE LASE. International Society for Optics and Photonics, pp 97410H–97410H-14
- Rappaz M, Drezet JM, Gremaud M (1999) A new hot-tearing criterion. *Metall Mater Trans A* 30A(2):449–455
- Liu J, Kou S (2016) Crack susceptibility of binary aluminum alloys during solidification. *Acta Mater* 110:84–94
- Kou S (2015) A criterion for cracking during solidification. *Acta Mater* 88:366–374
- Liu J, Kou S (2015) Effect of diffusion on susceptibility to cracking during solidification. *Acta Mater* 100:359–368
- Danis Y, Lacoste E, Arvieu C (2010) Numerical modeling of inconel 738LC deposition welding: prediction of residual stress induced cracking. *J Mater Process Technol* 210(14):2053–2061
- Ebrahimzadeh H, Mousavi SAAA (2012) Investigation on pulsed Nd:YAG laser welding of 49Ni–Fe soft magnetic alloy. *Mater Des* 38:115–123
- Hossain Ebrahimzadeh HF, Mousavi SAAA, Ghahramani A (2020) Microstructural analyses of aluminum-magnesium-silicon alloys welded by pulsed Nd:YAG laser welding. *Int J Miner Metall Mater*
- Zain-ul-Abdein M, Nelias D, Jullien J-F, Deloison D (2009) Prediction of laser beam welding-induced distortions and residual stresses by numerical simulation for aeronautic application. *J Mater Process Technol* 209(6):2907–2917
- Masubuchi K (1980) Chapter 3 - Fundamental information on residual stresses. In: Analysis of welded structures, Pergamon, pp 88–111
- Sheikhi M, Malek Ghaini F, Assadi H (2014) Solidification crack initiation and propagation in pulsed laser welding of wrought heat treatable aluminium alloy. *Sci Technol Weld Join* 19(3):250–255
- Kou S (2003) Welding metallurgy, 2nd edn. Wiley, New Jersey
- Al-Akel AS, Abdelatif AK, Gharbia FA (2002) Effect of preheating on hot cracking susceptibility of welded austenitic stainless steel. 5
- Hekmatjou H, Naffakh-Moosavy H (2018) Hot cracking in pulsed Nd:YAG laser welding of AA5456. *Opt Laser Technol* 103:22–32
- He X, Fuerschbach P, DebRoy T (2003) Heat transfer and fluid flow during laser spot welding of 304 stainless steel. *J Phys D Appl Phys* 36(12):1388
- He X, Elmer J, DebRoy T (2005) Heat transfer and fluid flow in laser microwelding. *J Appl Phys* 97(8):084909
- Nie F et al (2018) Microstructure and mechanical properties of pulse MIG welded 6061/A356 aluminum alloy dissimilar butt joints. *J Mater Sci Technol* 34(3):551–560
- Zhang J, Weckman DC, Zhou Y (2008) Effects of temporal pulse shaping on cracking susceptibility of 6061-T6 aluminum Nd:YAG laser welds. *Weld J* 87:18s–30s
- Mai TA, Spowage AC (2004) Characterisation of dissimilar joints in laser welding of steel–kovar, copper–steel and copper–aluminium. *Mater Sci Eng A* 374(1):224–233
- Ye X, Zhang P, Zhao J, Ma P (2018) Effect of macro- and micro-segregation on hot cracking of Inconel 718 superalloy argon-arc multilayer cladding. *J Mater Process Technol* 258:251–258
- Arivarasu M et al (2014) Micro-segregation studies on the continuous Nd: YAG laser beam welded AISI 316L. *Procedia Engineering* 97:892–901
- Praveen P, Yarlagadda P (2005) Meeting challenges in welding of aluminum alloys through pulse gas metal arc welding. *J Mater Process Technol* 164:1106–1112

Publisher's note Springer Nature remains neutral with regard to jurisdictional claims in published maps and institutional affiliations.